Extreme loads analysis of a site-specific semi-submersible type wind turbine

Xiaosen Xu[1)], Oleg Gaidai[2*)], Arvid Naess[3)], Prasanta Sahoo[1)]

[1)] *Florida Institute of Technology, Melbourne, USA*
[2)] *Jiangsu University of Science and Technology, Zhenjiang, China*
[3)] *Norwegian University of Science and Technology, Trondheim, Norway*

As a vital key part of the modern offshore wind energy industry, floating offshore wind turbines (FOWT) are built to generate green renewable energy. Robust prediction of extreme loads during FOWT operation is an important safety concern. In this paper, the FAST code has been used to analyze offshore wind turbine internal bending moments due to environmental hydrodynamic wave loads, acting on a specific FOWT under actual local sea conditions. This paper advocates a computationally efficient Monte Carlo based methodology for estimating extreme load or response statistics, based on simulations or measurements. For this purpose, the averaged conditional exceedance rate (ACER) method is proposed. The methodology provides for accurate extreme value prediction, representing an efficient use of all available data. In this study the estimated return level values, obtained by the ACER method, are compared to the corresponding return level values obtained by the Gumbel method. Based on the overall performance of the proposed method, it is concluded that the ACER method can provide more robust and accurate prediction of extreme structural loads. The described approach may be well used at the design stage, while defining optimal wind turbine parameters that would minimize potential FOWT mechanical damage due to excessive environmental loadings.

Keywords: Offshore wind turbine; extreme load statistics; Gumbel distribution;

ACER method;

[*)] Corresponding author Oleg Gaidai, Jiangsu University of Science and Technology, email: o_gaidai@just.edu.cn

1. Introduction

Wind energy is one of the most important renewable green energy resources, satisfying the drive of an expanding offshore energy industry. Offshore wind power, or offshore wind energy, is typically generated by wind farms constructed offshore, usually on the continental shelf, harvesting wind energy and generating electricity. Offshore wind speeds are typically stronger compared to those onshore, therefore offshore wind power contribution in terms of electricity supplied is of significant industrial importance.

Relatively low surface roughness of the ocean normally yields higher mean wind speeds. Recent developments within offshore wind turbines design have been obviously important for efficient generation of renewable energy. FOWTs are naturally exposed to turbulent wind flows and hydrodynamic loads, therefore their extreme load capacities are of significant engineering importance for FOWT design and operation.

There are usually two approaches for obtaining wind turbine design loads: (a) simulate events with rare occurrence that cause high load levels and are thus likely to be structural design drivers, and (b) simulate turbine response under normal operating conditions and extrapolate structural responses by fitting short-term probability distribution in its extreme tail (Dimitrov, 2016). Note that current study addresses long-term probability distribution. According to IEC 61400-1 standard (IEC, 2005), both approaches for obtaining extreme design loads may be recommended. This paper intends to contribute to the second approach (b), as being more statistically accurate as it utilizes full statistical distributions, and not a single extreme load/response event. This study therefore advocates methodology that has been already validated for a wide range of marine structures such as various offshore platforms and vessels (Gaidai et. al., 2018; Zhang et. al., 2019; Gaidai et. al., 2016; Naess et. al., 2010; Naess et. al., 2009; Naess

et. al., 2008; Naess and Moan, 2013). Figure. 1 presents an example of FOWT in offshore operation, similar to the one studied in this paper.

Figure. 1. An example of FOWT in offshore operation.

Numerous studies have been conducted, aiming at accurate estimation of ultimate loads within the framework of offshore wind turbines design. Fogle et. al. (2008) applied global maxima and block maxima for loads extrapolation of a wind turbine. Ernst and Seume (2012) used data from FINO research platform to investigate turbulent intensity and determined extreme loads of a 5 MW wind turbine using a peak over threshold extrapolation method. Dimitrov (2016) compared four extrapolation techniques applied to wind turbine environmental loads. Li et. al. (2015) developed a MATLAB code for dynamic analysis of a semi-submersible type of floating wind turbine. Graf et al. (2016) evaluated the long-term fatigue loads of a floating wind turbine by using Monte Carlo method. Aggarwal et al. m(2017) studied the nonlinear short-term extreme responses of a spar-type floating wind turbine. Li et. al. (2018) studied effects of simulation length on accumulated fatigue damage.

This paper aims at efficient use of simulated or measured structural data; for that purpose the averaged conditional exceedance rate (ACER) method has been adopted. The available structural load statistics is combined with a suitable class of parametric functions for describing the tail behavior of the extreme value distribution. Next, a comprehensive procedure for estimation of extreme values is obtained, that is not based on the assumption of a purely asymptotic distribution of the extreme values. This assumption is a distinctive feature of classical methods like Gumbel, Pareto, Weibull, peaks-over-threshold (POT) and other commonly used engineering techniques.

In other words, the ACER method does not incorporate the generalized extreme value distribution (GEV) concept, which makes the ACER method more flexible to tackle real-life data sets which are never truly asymptotic. This inconsistency between the imposed asymptotic behavior on real-life nonasymptotic data has occasionally lead to grave errors in the predicted long return period design values.

A clear engineering design advantage of the advocated approach, compared to e.g. a direct Monte Carlo method, is that much less simulations or measurements are needed to obtain equally accurate extreme value estimates.

2. Environmental conditions

High-quality metocean data with high temporal resolution is often difficult to find. The data source for this project was the National Oceanic and Atmospheric Administration (NOAA). The NOAA organization maintains an extensive network of floating data-collection buoys scattered throughout US and international waters. Data from these buoys can be found at the National Data Buoy Center (https://www.ndbc.noaa.gov/).

The first step in this study was to download the data from the NOAA website.

To ensure statistical significance of the data, only sites with at least 5 years of data were selected for processing. The selected sites also needed to include five measurement signals that were deemed necessary for offshore wind energy applications: mean wind speed, significant wave height, wave peak-spectral period, wind direction and wave direction. As the purpose of this paper is rather illustratory, only three major measurement signals have been chosen, that is however is not a limitation of the suggested approach. Requirements for a wave direction measurement proved to be the most limiting, leading to 23 offshore sites that met all criteria. Figure. 2 shows locations and names of selected from the NOAA database sites.

The data was collected and processed in different ways from different device sensors. The wind speed data was averaged over 8 min and reported hourly. The wind direction was averaged per direction with the same 8 min averaging period. The significant wave height was measured as the average height of the highest one-third of waves over a 20 min period, reported every hour.

Peak-spectral period was the wave period with the maximum wave energy over this same 20 min wave measurement period. Wave direction was reported as the direction from which waves at the dominant period arrived.

National Data Buoy Center Station Cape Elizabeth was finally selected for the present research. The measurement buoy was located 45 nautical miles Northwest of Aberdeen, Washington; it was located near the continental shelf edge at 125 m of water depth. Figure. 2 presents US National Data Buoy Centre stations along with Cape Elizabeth location marked in red (Stewart et. al., 2016). Joint wind-wave statistics for the above-mentioned location was estimated from the in situ measured metocean hourly historical data during 2010-2017 years.

Figure. 2. US National Data Buoy Center stations. Cape Elizabeth is indicated in red.

Figure. 3 presents a flow chart for the Monte Carlo based long term statistical analysis utilized in this paper. Note that by "sea state" the authors imply the full set of accounted environmental conditions, including wind speed. As already mentioned, only the National Data Buoy Center Station Cape Elizabeth was selected for the present research.

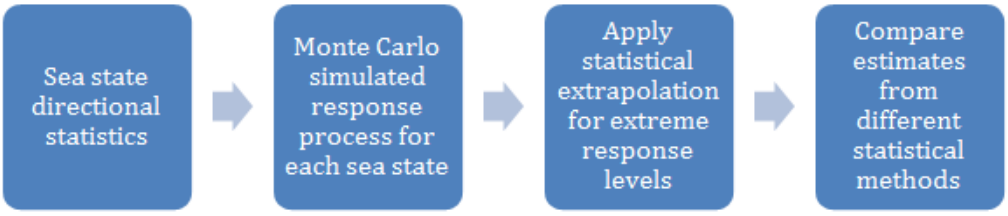

Figure. 3. Flow chart for described long term statistical analysis.

Post-processing of the data then continued with the extrapolating of the wind speed to a typical FOWT hub height of 90 m. The anemometers of Cape Elizabeth are placed at 5 m above sea level. Most engineering approaches use either log law or power law wind shear equations for the extrapolation, which can be seen in Eqs (1) and (2), respectively:

$$U(z) = U(z_r)\frac{ln(z)-ln(z_0)}{ln(z_r)-ln(z_0)} \quad (1)$$

$$U(z) = U(z_r)\left(\frac{z}{z_r}\right)^{\alpha} \quad (2)$$

with $U(z)$, $U(z_r)$ being the wind speed at height z and the reference wind speed at height z_r respectively. z_0 is the surface roughness length and α is the power law constant. In this paper the power law given by Eq. (2) has been preferred with α=0.14. For this study, the following conditionalities are used, as defined in the design standards:

- Wind speed U
- Significant wave height H_s
- Peak-spectral period T_p

In this paper a scatter diagram approach was adopted, namely the measured buoy data has been post-processed into an empirical multi-dimensional joint distribution, without any simplifications or assumptions. More specifically, the empirical joint probability density function (PDF) $p(U, H_s T_p)$ has been estimated directly from the available metocean data, resulting in a three dimensional scatter diagram. Since the wind/wave misalignment has not been an input parameter for FAST simulation, only the three-dimensional probability space $(U, H_s T_p)$ has been adopted. Note that the described approach is well suited for higher dimensional scatter diagrams. Figure. 4 presents on the left: In situ wind speed versus significant wave height correlation pattern; on the right: (H_s, T_p) contour plot, $p(H_s T_p) = \int p(U, H_s T_p)\, dU$.

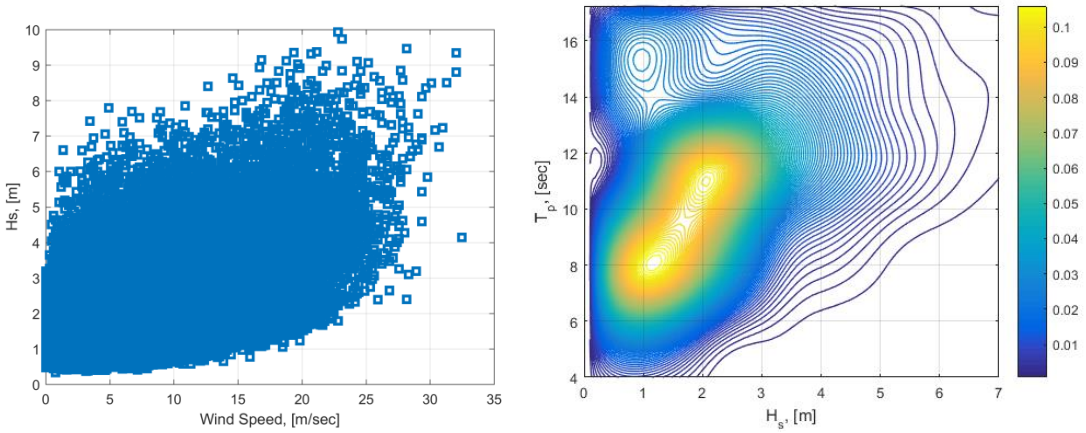

Figure. 4. Left: In situ wind speed versus significant wave height correlation pattern; Right: (H_s, T_p) contour plot of the joint probability density $p(H_s\, T_p) = \int p(U,\, H_s\, T_p)\, dU$.

The above described approach can be regarded as a direct Monte Carlo long term simulation approach, which has the advantage of not incorporating various simplifications and assumptions, like e.g. Stewart et. al. (2016), where the wind speed was considered as an independent parameter (typical in many FOWT engineering applications). Note that Figure. 4, on the left, exhibits a clear correlation between wind speed U and significant wave height H_s. Therefore, it is not always accurate to assume wind speed as an independent parameter. Note that this paper is not aiming at quantifying e.g. environmental correlation patterns, but rather at a qualitative study that advocates using scatter distributions without simplifications. An advantage of avoiding over-simplification of the empirical multi-dimensional probability distribution function (PDF) is highlighted by Figure. 4.

For the current study, the total 12 different wind speed bins have been selected, ranging from 3 to 25 m/sec. For each wind speed bin (U), about 30 corresponding sea states (H_s, T_p) with different probabilities have been selected for further numerical simulation. In this way, the scatter diagram three dimensional probability distribution $p(U,\, H_s\, T_p)$ has been properly taken into account within a frame of Monte

Carlo simulated data sets. For details on how the ACER functions corresponding to different short term wind-sea states are combined into one long term ACER function, $ACER_k(\eta)$, with η being the response (or load) level of interest, see Appendix Eq. (5A).

Note that this study has relied on the NOAA buoy data, with subsequent application of a scatter diagram approach to get the empirical multi-dimensional PDF. The authors did not compare the resulting PDF to PDFs from satellite data, since this study is focusing on an approach of fully using distributions derived from scatter diagrams without simplifications, rather than aiming at producing quantitative engineering numerical values.

3. Model description in brief

The DeepCwind semi-submersible type supporting platform, namely OC4 semi-submersible floating system of Robertson et. al. (2014) has been chosen for the current study. Figure. 5 shows the model of the semi-submersible platform, which consists of one main column and three outer offset columns. There are heave plates (base columns) attached to the bottom in order to reduce large heave motions.

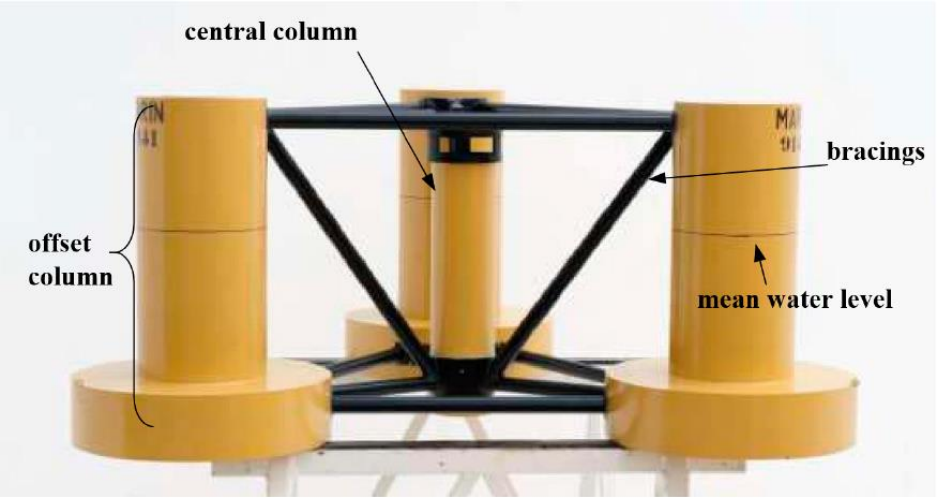

Figure.5. 1/50 scale model of the DeepCwind semi-submersible platform.

Table 1 presents the main dimensions of the full scale semi-submersible platform.

Table 1. Main dimensions of the semi-submersible platform.

Item	Value
Platform draft	20.0 m
Spacing between offset columns	50.0 m
Length of upper columns	26.0 m
Length of base columns	6.0 m
Diameter of central column	6.5 m
Diameter of offset (upper) columns	12.0 m
Diameter of base columns	24.0 m

The NREL 5-MW baseline wind turbine is placed on top of the OC 4 semi-submersible platform. The diameter of the three-bladed rotor is 126 m and the hub height of the cylindrical tower is 90 m. Table 2 summarizes properties of the 5-MW baseline wind turbine.

Table 2. Summary properties of 5-MW baseline wind turbines.

Item	Value
Rotor orientation	Upwind, 3 blades
Cut-in/Rated/Cut-out wind speed	3 m/s, 11.4 m/s, 25 m/s
Rotor mass	110,000 kg
Nacelle mass	240,000 kg
Tower mass	347,460 kg
Hub height	90 m

FAST and AeroDyn account for applied aerodynamic and gravitational loads, enabling accurate numerical estimation of the wind turbine structural dynamics. The

FAST software include various mechanical effects such as e.g. elasticity of the rotor tower, along with the elastic coupling between their motions and the motions of the support platform as well as dynamic coupling between the support platform motions and of the wind turbine motions. FAST employs a combined modal and multibody structural dynamics formulation, see Jonkman et. al. (2005).

Numerical simulations for the current study were run with a sufficient number of degrees-of-freedom (DOFs), including FAST two flap wise and one edgewise mode DOFs per blade, one drivetrain torsion DOF, one variable generator-speed DOF, one nacelle yaw DOF, two fore-aft and two side-to-side tower mode DOFs, as well as floating system DOFs, namely three translational (surge, sway, and heave) and three rotational (roll, pitch, and yaw) DOFs of the platform, see Jonkman et. al. (2007).

4. Dynamic analysis of wind turbine simulations

In the present study, the aero-hydro-servo-elastic simulation code FAST Jonkman et. al. (2005) was used to simulate various coupled system responses. Stochastic wind fields are generated by TurbSim Jonkman (2009) on a 31×31 square grid with 145 m width. AeroDyn, which is the FAST code module, was able to model aerodynamics of baseline wind turbines using the blade element momentum method with proper consideration of rotor-wake effects and dynamic stall. Hydrodynamic loads were modelled by FAST HydroDyn Jonkman et. al. (2014) module, which incorporates Morison's equation aimed at slender structures and potential flow theory suitable for large-diameter structures. The drag force term in Morison's equation accounted for viscous drag forces acting on FOWT. The second-order wave forces have been taken into account in FAST numerical simulation as well, see Bayati et. al. (2014). According to IEC-61400-1 from the International Electro technical Commission (2005), at least 15

short term simulations of 10 minute duration were required for ultimate loads extrapolation, aiming at 50-year return period under normal production conditions. Based on IEC-61400-3 from the International Electro technical Commission (2009), Design Load Case (DLC) 1.1, for the current study the total of 2550 times 10 min short term random realizations have been numerically simulated, with cut-in wind speed 3 m/s and cut-out wind speed 25 m/s; wind speed scatter diagram bin size has been set to 2 m/s. The total length of each simulation was set to 800 sec with first 200 sec being removed from post processing due to initial transient effects. Figure. 6 shows a sample time series of the tower base fore-aft bending moment and platform pitch. The mean value of the tower base fore-aft bending moment is non-zero because of the wind turbine thrust force and is proportional to the wind turbine thrust force. It indicates that ultimate structural loads are more likely to reach a certain extreme level when subject to large wind forces. Besides, the obvious fluctuating component is observed, and therefore the ultimate structural loads are determined by both aerodynamic and hydrodynamic excitation.

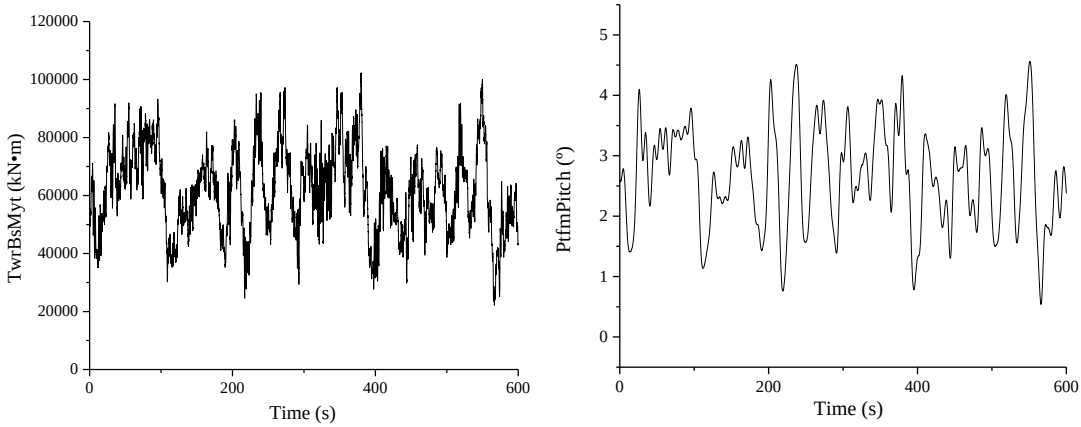

Figure. 6. Sample time series of tower base fore-aft bending moments and platform pitch when $U_{hub} = 11\mathrm{m/s}$.

Extensive experimental work of OC4 and OC5 projects have been conducted in order to provide experimental data which is useful in validating floating offshore wind turbine modelling tools, see e.g. Coulling et. al. (2013) and Benitz, et. al. (2015). The average error with respect to experimental results across OC5 FAST numerical results was about 10% under-prediction of the tower top ultimate shear load; about 14% under-prediction for the tower-base load; about 20% under-prediction of the upwind mooring tension for wave-only cases, see Robertson et. al. (2017). The experimental validation results give the authors confidence in using FAST as a numerical simulation tool for the current study.

5. Extreme load analysis

This section, together with the Appendix, presents extreme value analysis results, which include the results obtained by the proposed ACER method, as well as Gumbel method predictions for comparison. The basic extreme value distribution provided by the ACER method can be written as follows,

$$P(\eta) \approx \exp(-(N-k+1)\,\mathrm{ACER}_{\mathrm{k}}(\eta)), \tag{3}$$

where $\mathrm{ACER}_{\mathrm{k}}(\eta)$ denotes the ACER function of order k, and where N denotes the total number of data points in the time series analyzed. The ACER function expresses a conditional exceedance rate, which is extracted from the measured or simulated time series as detailed in the Appendix. A plot of the ACER functions will reveal the effect of statistical dependence between sampled data points in the time series. By studying the ACER plot, it may be decided what order is needed to obtain a good approximation to the extreme value distribution inherent in the data.

Fig. 7 presents convergence diagnostics for the $\mathrm{ACER}_{\mathrm{k}}$ functions for the out-of-plane blade root bending moment. Note that this diagnostic plot has been based on a time

series of sampled peak values. The practical consequence of this is that the peak values are considered independent for k = 1, which would yield similar results as the well-known Poisson assumption, which is known for its accuracy in the absence of narrow band effects in the response process. For k > 1, dependence effects are taken into account with an accuracy that increases with increasing k. It is interesting to observe from the diagnostic plot of Fig. 7 that already k = 2 captures most of the dependence effects on the ACER function. A prerequisite for this observation is that the time series consist of local peak values. Fig. 7 also shows that the ACER_{10} function, i.e. with the conditioning level $k = 10$, provides a good candidate for deep tail estimation.

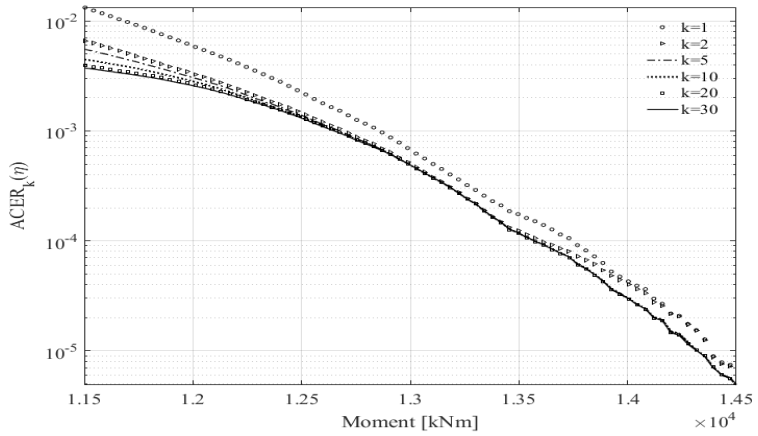

Figure. 7 ACER_k functions convergence diagnostics for the out-of-plane blade root bending moment.

Fig. 8 presents the 50 years predicted response level along with 95% CI for the out-of-plane blade root bending moment, note over-estimation of predicted response by Gumbel method. Note that extrapolation has different cut on markers η_* for different channels, therefore the accuracy of extrapolation and CI width differ. In other words, different responses exhibit different quality of fitting. The cut on tail markers η_* is the smallest (left) value on the horizontal axis on the ACER_k (left) in Fig 8 and Fig 10; see Appendix Eq. (7A) for the tail marker definition.

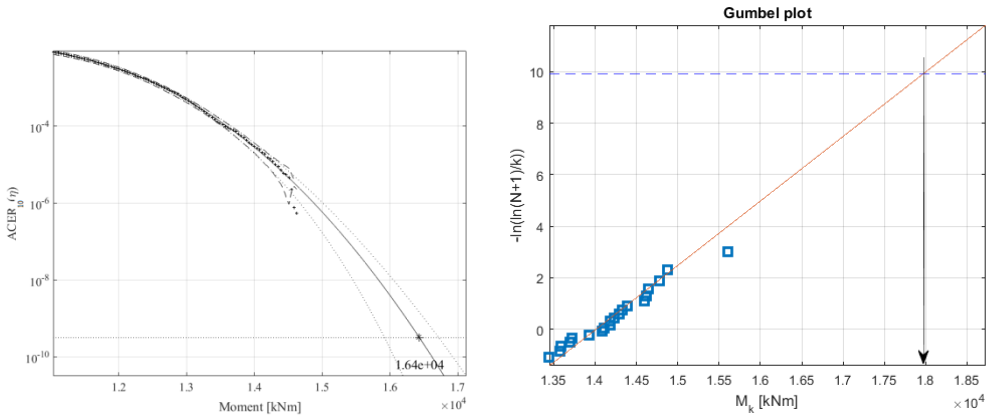

Figure. 8 Left: Blade root bending moment out-of-plane, 50yr predicted bending moment level. Stars (*) indicate $ACER_5$ values, dashed lines (--) indicate 95% CI, horizontal line indicates 50 yrs level of interest; solid lines indicate extrapolated $ACER_{10}$ and CI. Right: Gumbel fit. Scatter diagram probabilities set equal in both cases.

Fig. 9 presents convergence diagnostics for the $ACER_k$ functions for the anchor tension with conditioning level *k* running up to 30. This covers most of the characteristic time constants of the dynamics of the floater, which is the determining factor for the anchor forces. Note that conventional Gumbel fit does not account for scatter diagram probabilities, i.e. all maxima are expected to have equal probability. Therefore in this paper for the Gumbel fit, all analysed sea states were considered to be equally probable (i.e. neglecting scatter diagram probabilities).

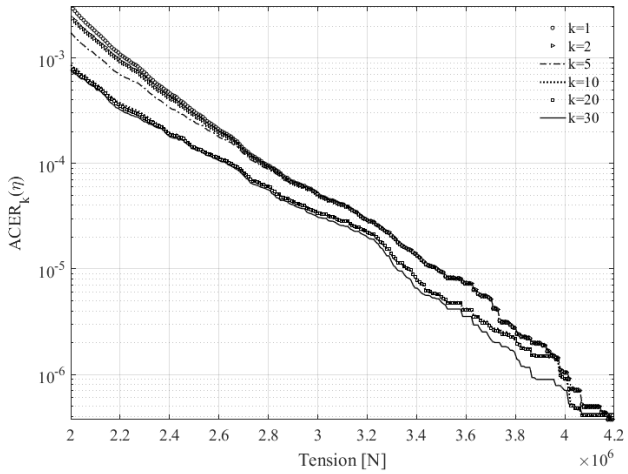

Figure. 9 $ACER_k$ functions convergence diagnostics for the anchor tension.

Note again that individual local peaks have been extracted for $ACER_k$ estimation. Since the original simulated time series used a time increment $dt = 0.2$ sec, it was observed that on the average 10 discrete time steps with length of dt would correspond to the time between local peaks. Therefore, the average time lapse between neighbouring local peaks in $ACER_k$ estimation was 2 seconds. Thus, $ACER_{10}$ for the anchor tension local peak data would cover 20 seconds of declustering time span.

For the anchor tension, the conditioning level k for $ACER_k$ has been chosen to be equal 10, according to a similar study as in Fig 7. Note that the necessity of a higher conditioning level k signals the presence of stronger narrow band effects, as is indeed the case for tensile loads.

In Fig. 10 is shown the predicted 50 yr anchor tension level, 50 yr. Note that the ACER function tail in Fig. 10 on the left exhibits an almost straight line behaviour, as opposed to the concave shape in Fig. 8. This rather fat tailed distribution is typical for tensile loads, see for example the tether tension measured for a tension leg platform (TLP), see Teigen et. al. (2006), Næss et. al. (2007a), Næss et. al. (2007b), where the ACER functions become even markedly convex. Of course, a global straight line in an ACER plot corresponds to a Gumbel distribution. Therefore, in this specific case, the ACER and Gumbel methods provide almost identical answers. Typically, the Gumbel distribution would only show up as an asymptotic limiting distribution, but in this specific case the ACER plot convincingly reveals that the Gumbel distribution is indeed a good global approximation.

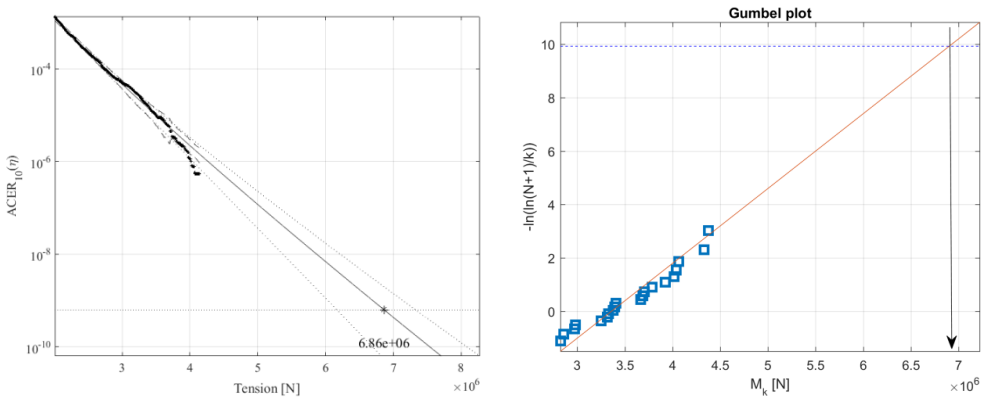

Figure 10. Left: Anchor tension, 50yr predicted tension level. Stars (*) indicate $ACER_{10}$ values, dashed lines (--) indicate 95% CI, horizontal line indicates 50 yrs level of interest; solid lines indicate extrapolated $ACER_{10}$ and CI. Right: Gumbel fit. Scatter diagram probabilities set equal in both cases.

Note good agreement between ACER and Gumbel methods for predicted response level in Fig. 10. Table 1 presents various predicted FOWT response values for 20 and 50 years return periods.

Table 1 Various predicted FOWT load values for 20 and 50 years return periods. Scatter diagram probabilities set unequal/equal.

	20 years return period	50 years return period
Out-of-plane bending moment	16.01/16.35MN·m	16.21/16.43 MN·m
Tower-base side-to-side bending moment	37.91/38.64 MN·m	38.71/39.62 MN·m
Tower-base fore-aft bending moment	170.61/173.11 MN·m	173.23/176.02 MN·m
Anchor tension	6.25/ 6.58 MN	6.72/6.86 MN

Regarding the comparison between the proposed ACER method and the Gumbel fit, it was found that although both estimates are within 95% CI of each other, the Gumbel fit yields about five times wider CI than ACER, if CI width is measured relatively to the predicted value itself. Regarding validation of the proposed method versus direct Monte Carlo simulation, the total simulation length was reduced 100 times. The extreme value prediction obtained by the ACER method was in a proper agreement with direct Monte Carlo simulation of the full length (not reduced 100 times). This shows

that the ACER method is at least 100 times more efficient than direct Monte Carlo simulation, making the proposed approach an attractive CPU saving engineering option.

Regarding the relative simulation time of post-processing long term simulation results by the ACER method, compared to the FAST method, it is noted that the ACER method virtually took no computational effort, compared to the main FAST computational effort.

6. Results and conclusions

This study focused on the FOWT subjected to extreme environmental loads during operation, provided by Cape Elizabeth metocean conditions. In particular, various structural FOWT bending moments have been numerically simulated.

One method to obtain load design values is the classical Gumbel method, which is based on adopting an asymptotic extreme value distribution. An alternative approach is a state-of-the-art method called the ACER method, which is based on a generalization of the Gumbel type extreme value distribution in combination with non-parametric ACER functions. The ACER method is implemented by expressing the extreme value distribution in terms of an empirical average conditional exceedance rate function. By fitting a parametric function to the empirical exceedance rate, it is shown that the tail behaviour of the empirical extreme value distribution can be quite accurately captured. The ACER method has been validated by application to a wide range of simulation models, and, in general, very accurate predictions were obtained, cf. Naess et. al. (2008, 2009, 2010, 2013); Gaidai et. al. (2016, 2018); Jian et. al. (2018).

It is shown that the asymptotic assumption, needed by conventional methods like the Gumbel method, may not be fully applicable to the analysed data set, i.e. the data are not extreme enough. The ACER method, on the other hand, does not rely on

assuming asymptotic data.

The accuracy of the ACER method was found to be more than twice better than the Gumbel one, based on a comparison of the ratio (confidence interval width)/(predicted value).

Finally, the presented methodology has the following important advantages:

- Any kind of FOWT response data can be analysed: either numerically simulated or measured.
- Unlike asymptotic methods (Gumbel, Weibull, Pareto etc.), the presented method can be called pre-asymptotic, which means that the data set can be analysed more accurately and efficiently.
- The presented method yields about four times narrower confidence interval, than a Gumbel based method, for the predicted FOWT loads.
- The proposed methodology conveniently incorporates sea state environmental scatter diagrams, unlike other conventional methods, e.g. Gumbel.

7. Appendix

For a stationary or nonstationary stochastic process $Z(t)$, that has been simulated over a certain time interval $(0, T)$, there are typically discrete process values $X_1, \dots, X_N$, that have been measured/simulated at equidistant time moments $t_1, \dots, t_N$ in $(0, T)$. The discrete process values could be exactly observed/calculated values of $X(t)$ at each $t_j, j = 1, \dots, N$, or it could be maxima values over time intervals centered at the t_j's. The target is to accurately estimate the cumulative distribution function (CDF) of the extreme value $M_N = \max\{X_j ; j = 1, \dots, N\}$. It is of interest to estimate $P(\eta) =$

$\text{Prob}(M_N \leq \eta)$ for large values of η. The following random functions are introduced Naess and Gaidai (2009)

$$A_{kj}(\eta) = \mathbf{1}\{X_j > \eta, X_{j-1} \leq \eta, \dots, X_{j-k+1} \leq \eta\}, \quad j = k, \dots, N, k = 1, 2, 3, \dots, N \tag{1A}$$

and

$$B_{kj}(\eta) = \mathbf{1}\{X_{j-1} \leq \eta, \dots, X_{j-k+1} \leq \eta\}, \quad j = k, \dots, N, k = 1, 2, 3, \dots, N \tag{2A}$$

where $\mathbf{1}\{\mathcal{A}\} = 1$ if $\mathcal{A}$ is true, while it is zero if not. For k = 1, 2, …, define the statistical distribution functions (CDFs)

$$P_k(\eta) = \exp\left(-\sum_{j=k}^{N} \frac{\mathbb{E}[A_{kj}(\eta)]}{\mathbb{E}[B_{kj}(\eta)]}\right) \approx \exp\left(-\sum_{j=k}^{N} \mathbb{E}\left[A_{kj}(\eta)\right]\right), \quad \eta \to \infty \tag{3A}$$

As shown in Naess et. al. (2009), $P_k(\eta) \to P(\eta)$, as k increases. It is assumed that the long term response time series can be sub-divided into K blocks such that $\mathbb{E}[A_{kj}(\eta)]$ remains approximately constant within each block and such that $\sum_{j \in C_i} \mathbb{E}\left[A_{kj}(\eta)\right] \approx \sum_{j \in C_i} a_{kj}(\eta)$ for a sufficient range of η-values, where C_i denotes the set of indices for block with number i; with $i = 1, \dots, K$, and where $a_{kj}(\eta)$ are the realized values of $A_{kj}(\eta)$ for the simulated (or measured) time series, then $\sum_{j=k}^{N} \mathbb{E}\left[A_{kj}(\eta)\right] \approx \sum_{j=k}^{N} a_{kj}(\eta)$. Typically, each block would then consist of data from identical short term sea states within the long term time series. Thus, it is obtained that,

$$P_k(\eta) \approx \exp\left(-(N-k+1)\hat{\varepsilon}_k(\eta)\right), \; \hat{\varepsilon}_k(\eta) = \frac{1}{N-k+1}\sum_{j=k}^{N} a_{kj}(\eta), \tag{4A}$$

where the empirical (long term) ACER function of order k, $\hat{\varepsilon}_k(\eta)$, has been defined. Alternatively, for easy identification, $\hat{\varepsilon}_k(\eta)$ is also denoted as $\mathrm{ACER_k}(\eta)$.

Now, consider a scatter diagram of $m = 1,..,M$ sea states, each sea state having probability p_m, so that $\sum_{m=1}^{M} p_m = 1$. The long term ACER function may then be expressed as,

$$\hat{\varepsilon}_k(\eta) = \sum_{m=1}^{M} \hat{\varepsilon}_k(\eta, m)\, p_m \,, \tag{5A}$$

where $\hat{\varepsilon}_k(\eta, m)$ is the same function as in Eq. (4A), but corresponding to a specific sea state with number m. Each sea state of the scatter diagram would then correspond to a block in the discussion above. As shown in Naess et. al. (2009), the long term extreme value distribution of $M(T)$, based on the ACER function of order k, can then be expressed as follows,

$$P(\eta) \approx \exp(-(N - k + 1)\, \hat{\varepsilon}_k(\eta)) \tag{6A}$$

where $\hat{\varepsilon}_k(\eta)$ is the empirical ACER function derived from Eq. (4A) or (5A) with $k \ll N$, where N is the total number of data points in the time series analysed.

The choice of what value of k to use in a specific case, depends on the dependence structure of the time series. For instance, if the response time series contains contributions from several narrow band modal responses, it is important to choose k large enough to cover a time span exceeding the longest characteristic time of the dynamics, which would typically be associated with the lowest spectral peak of the response spectrum. With such information available, it can then be decided whether f.ex. $k = 2$ can be used as a good approximation.

As the order k increases, the accuracy of Eq. (6A) improves, but the amount of data for $\hat{\varepsilon}_k(\eta)$ estimation gets gradually less. Results from Section 5 of this paper show

that the $\hat{\varepsilon}_k(\eta)$ functions converge conveniently fast with growing k, see (Naess et. al. 2009; Naess et al. 2010).

The $\hat{\varepsilon}_k(\eta)$ as functions of the response level η are in general quite regular in the tail, i.e. for high values of η. More specifically, for $\eta \geq \eta_0$, the tail behaves very closely like $\exp\{-a(\eta-b)^c+d\}$ with a, b, c, d being suitable constants for an appropriate threshold η_0. This is based on the underlying assumption that the domain of attraction of the extreme value distribution belongs to the asymptotic Gumbel case.

The optimization on the log-level was done by minimizing the following mean square error function F with respect to the four arguments a_k, b_k, c_k, d_k,

$$F(a_k, b_k, c_k, d_k) = \int_{\eta_0}^{\eta_1} \omega(\eta)\{\ln(\hat{\varepsilon}_k(\eta)) - (a_k(\eta-b_k)^{c_k} - d_k)\}^2 d\eta, \qquad \eta \geq \eta_0 \qquad (7A)$$

where η_1 is a suitable data cut-off value, i.e. the largest response value where the confidence interval width can be calculated. The weight function ω was defined as $\omega(\eta)=\{\ln C^+(\eta) - \ln C^-(\eta)\}^{-2}$ with $\left(C^-(\eta),\ C^+(\eta)\right)$ being a 95% confidence interval (CI), empirically estimated from the simulated data. The procedure for optimizing the parameters a_k, b_k, c_k, d_k was outlined in (Naess et. al. 2009; Naess et. al. 2010; Naess and Gaidai 2008; Naess and Gaidai 2009).

8. References

Aggarwal N, Manikandan R, Saha N. 2017. Nonlinear short term extreme response of spar type floating offshore wind turbines. Ocean Eng. 130:199–209.

Bayati, I., Jonkman, J., Robertson, A., Platt, A. (2014). "The effects of second-order hydrodynamics on a semi-submersible floating offshore wind turbine." In Journal of Physics: Conference Series (Vol. 524, No. 1, p. 012094). IOP Publishing.

Benitz, M. A., Schmidt, D. P., Lackner, M. A., Stewart, G. M., Jonkman, J., Robertson, A. (2015). "Validation of hydrodynamic load models using CFD for the OC4-DeepCwind semi-submersible." National Renewable Energy Lab.(NREL), Golden, CO (United States).

Coulling, A. J., Goupee, A. J., Robertson, A. N., Jonkman, J. M., Dagher, H. J. (2013). "Validation of a FAST semi-submersible floating wind turbine numerical model with DeepCwind test data." Journal of Renewable and Sustainable Energy, 5(2), 023116.

Dimitrov, N. (2016). Comparative analysis of methods for modelling the short-term probability distribution of extreme wind turbine loads. Wind Energy, 19(4), 717-737.

Ernst, B., Seume, J. R. (2012). Investigation of site-specific wind field parameters and their effect on loads of offshore wind turbines. Energies, 5(10), 3835-3855.

Fogle, J., Agarwal, P., Manuel, L. (2008). Towards an improved understanding of statistical extrapolation for wind turbine extreme loads. Wind Energy: An International Journal for Progress and Applications in Wind Power Conversion Technology, 11(6), 613-635.

Gaidai, O., Cheng, Y., Xu, X., & Su, Y. (2018). Long-term offshore Bohai bay Jacket strength assessment based on satellite wave data. Ships and Offshore Structures, 13(6), 657-665.

Gaidai, O., Storhaug, G., & Naess, A. (2016). Extreme value statistics of large container ship roll. Journal of Ship Research, 60(2), 92-100.

Gaidai, O., Ji, C., Kalogeri, C., Gao, J. (2017). SEM-REV energy site extreme wave prediction, Renewable Energy, Vol 101, pp. 894-899.

Graf, P. A., Stewart, G., Lackner, M., Dykes, K., & Veers, P. (2016). High‐throughput computation and the applicability of Monte Carlo integration in fatigue load estimation of floating offshore wind turbines. Wind Energy, 19(5), 861-872.

International Electrotechnical Commission. (2005). IEC 61400-1: Wind turbines part 1: Design requirements. International Electrotechnical Commission, 177.

International Electrotechnical Commission. (2009). IEC 61400-3 Wind Turbines Part3: Design Requirements for Offshore Wind Turbines. International Electrotechnical Commission: Geneva, Switzerland.

Jian, Z., Gaidai, O., & Gao, J. (2018). Bivariate Extreme Value Statistics of Offshore Jacket Support Stresses in Bohai Bay. Journal of Offshore Mechanics and Arctic Engineering, 140(4), 041305.

Jonkman, J. M., Buhl Jr, M. L. (2005). "FAST user's guide." National Renewable Energy Laboratory, Golden, CO, Technical Report No. NREL/EL-500-38230.

Jonkman, J. M., Buhl Jr, M. L. (2007), "Loads Analysis of a Floating Offshore Wind Turbine Using Fully Coupled Simulation" WindPower 2007 Conference & Exhibition.

Jonkman, B. J. (2009). "TurbSim user's guide: Version 1.50 (No. NREL/TP-500-46198)." National Renewable Energy Lab. (NREL), Golden, CO (United States).

Jonkman, J. M., Robertson, A., Hayman, G. J. (2014). "HydroDyn user's guide and theory manual." National Renewable Energy Laboratory.

Li, L., Hu, Z., Wang, J., Ma, Y. (2015). Development and validation of an aero-hydro simulation code for offshore floating wind turbine. J. Ocean Wind Energy, 2(1), 1-11.

Li, H., Hu, Z., Wang, J., Meng, X. (2018). "Short-term fatigue analysis for tower base of a spar-type wind turbine under stochastic wind-wave loads." International Journal of Naval Architecture and Ocean Engineering, 10(1), 9-20.

Naess, A., & Gaidai, O. (2008). Monte Carlo methods for estimating the extreme response of dynamical systems. Journal of Engineering Mechanics, 134(8), 628-636.

Næss, A., & Gaidai, O. (2009). Estimation of extreme values from sampled time series. Structural Safety, 31(4), 325-334.

Naess, A., Gaidai, O., & Batsevych, O. (2010). Prediction of extreme response statistics of narrow-band random vibrations. Journal of Engineering Mechanics, 136(3), 290-298.

Naess, A., Stansberg, C. T., Gaidai, O., & Baarholm, R. J. (2009). Statistics of extreme events in airgap measurements. Journal of Offshore Mechanics and Arctic Engineering, 131(4), 041107.

Naess, A., & Moan, T. (2013). Stochastic dynamics of marine structures. Cambridge University Press.

Robertson, A., Jonkman, J., Masciola, M., Song, H., Goupee, A., Coulling, A., & Luan, C. (2014). Definition of the semisubmersible floating system for phase II of OC4 (No. NREL/TP-5000-60601). National Renewable Energy Lab.(NREL), Golden, CO (United States).

Robertson, A. N., Wendt, F., Jonkman, J. M., Popko, W., Dagher, H., Gueydon, S., ... & Soares, C. G. (2017). OC5 project phase II: validation of global loads of the DeepCwind floating semisubmersible wind turbine. Energy Procedia, 137, 38-57.

Stewart, G. M., Robertson, A., Jonkman, J., & Lackner, M. A. (2016). The creation of a comprehensive metocean data set for offshore wind turbine simulations. Wind Energy, 19(6), 1151-1159.

Naess, A., Gaidai, O., Teigen, P. (2007a), Extreme response prediction for nonlinear floating offshore structures by Monte Carlo simulation. Applied Ocean Research 2007, Vol. 29.(4) p. 221-230.

Naess, A., Gaidai, O., Teigen, P. (2007b), Simulation based estimation of extreme response of floating offshore structures. I: Proceedings of the 26th International Conference on Offshore Mechanics and Arctic Engineering. ASME Press, ISBN 0791837998.

Teigen, P., Gaidai, O., Naess, A., (2006), Springing Response Statistics of Tethered Platforms in Random Waves. Proceedings 25th International Conference on Offshore Mechanics and Arctic Engineering. ASME Press, ISBN 0791837777.